Non-CG methylation and multiple epigenetic layers associate child abuse with immune and small GTPase dysregulation

Pierre-Eric Lutz[1,†*], Marc-Aurèle Chay[1,*], Alain Pacis[2], Gary G Chen[1], Zahia Aouabed[1], Elisabetta Maffioletti[3], Jean-François Théroux[1], Jean-Christophe Grenier[2], Jennie Yang[1], Maria Aguirre[4], Carl Ernst[1,5], Adriana Redensek[6], Léon C. van Kempen[4], Ipek Yalcin[7], Tony Kwan[6], Naguib Mechawar[1,5], Tomi Pastinen[6,#] and Gustavo Turecki[1,5]

Affiliations:

[1] McGill Group for Suicide Studies, Douglas Mental Health University Institute, McGill University, Montréal, Canada

[†] Current address: Centre National de la Recherche Scientifique, Institut des Neurosciences Cellulaires et Intégratives, Université de Strasbourg, Fédération de Médecine Translationnelle de Strasbourg, Strasbourg, France

[2] Department of Genetics, CHU Sainte-Justine Research Center, Montréal, Canada

[3] Genetics Unit, IRCCS Istituto Centro San Giovanni Fatebenefratelli, Brescia, Italy

[4] Segal Cancer Centre, Lady Davis Institute, Jewish General Hospital, McGill University, Montréal, Canada

[5] Department of Psychiatry, McGill University, Montréal, Canada

[6] Department of Human Genetics, McGill University, Montréal, Canada

[#] Current address: Center for Pediatric Genomic Medicine, University of Missouri-Kansas City School of Medicine, Kansas City, USA

[7] Centre National de la Recherche Scientifique, Institut des Neurosciences Cellulaires et Intégratives, Université de Strasbourg, Fédération de Médecine Translationnelle de Strasbourg, Strasbourg, France

*, equal contribution

Correspondence should be addressed to:

Gustavo Turecki MD PhD

McGill Group for Suicide Studies

Douglas Mental Health Institute

Department of Psychiatry

McGill University

gustavo.turecki@mcgill.ca

Word count: main text, 4693; abstract, 149. References: 53.

7 Figures, 14 Supplementary Figures, 13 Supplementary Tables

Abstract

Early-life adversity (ELA), including child abuse and other forms of early-life maltreatment, is a major predictor of negative mental health outcomes. ELA is thought to increase lifetime risk of psychopathology by epigenetically regulating genomic regions that in turn adjust different brain systems. Here, focusing on the lateral amygdala, a major brain site for emotional homeostasis, we comprehensively describe molecular cross-talk across multiple epigenetic mechanisms, including 6 histone marks, DNA methylation and the transcriptome, in subjects with a history of ELA and healthy controls. We first provide evidence for previously unknown interactions among epigenetic layers in the healthy brain. Focusing on non-CG methylation, and particularly on CAC, our results further suggest that the immune system and small GTPase signaling are the most consistently impaired pathways in the amygdala of ELA individuals. Overall, the present work provides new insight into epigenetic regulation of brain plasticity as a function of early-life experience.

Introduction

Early-life adversity (ELA), including sexual and physical abuse, as well as other forms of child maltreatment, is a major public-health problem that affects children of all socio-economic backgrounds[1]. ELA is a strong predictor of increased lifetime risk of negative mental health outcomes, including depressive disorders[2]. Among other findings, a growing number of studies suggest an association between ELA and morphological and functional changes in the amygdala[3], a brain structure critically involved in emotional regulation[4]. It is possible, thus, that amygdala changes observed in individuals who experienced ELA may contribute to increase risk of psychopathology.

The amygdala is composed of inter-connected nuclei, among which the basal and lateral sub-divisions are responsible for receiving and integrating external information. In turn, these nuclei strongly innervate the central amygdala, the primary nucleus projecting outside the amygdalar complex to mediate behavioural outputs[4]. While specific functional properties of these nuclei remain difficult to assess in humans, animal studies indicate that the basal and lateral sub-divisions exhibit differential responsivity to stress, in particular as a function of the developmental timing of exposure (adolescence versus adulthood)[5, 6]. Here, we focused on homogeneous, carefully dissected tissue from the human lateral amygdala.

Childhood is a sensitive period, during which the brain is more responsive to the effect of life experiences[7]. Proper emotional development is contingent on the availability of a supportive caregiver, with whom children develop secure attachments[8]. On the other hand, ELA signals an unreliable environment that triggers adaptive responses, and deprives the organism from essential experience. A growing body of evidence now supports the hypothesis that epigenetic mechanisms play a major role in the persistent impact of ELA on gene expression and behaviour[9]. While DNA methylation has received considerable attention, available data also points towards histone modifications as another critical and possibly interacting factor[9]. Therefore, in this study we conducted a comprehensive characterization of epigenetic changes occurring in individuals with a history of severe ELA, and carried out genome-wide investigations of multiple epigenetic layers, and their cross-talk. Using post-mortem tissue from a well-defined cohort of depressed individuals with histories of ELA, and controls with no such history, we characterized 6 histone marks, DNA methylation, as well as their final endpoint at gene expression level.

We first generated data for six histone modifications: H3K4me1, H3K4me3, H3K27ac, H3K36me3, H3K9me3, and H3K27me3[10], using chromatin-immunoprecipitation sequencing (ChIP-Seq). This allowed us to create high-resolution maps for each mark, and to define chromatin states throughout the epigenome. In parallel, we characterized DNA methylation using Whole-Genome Bisulfite Sequencing (WGBS). While previous studies in psychiatry focused on the canonical form of DNA methylation that occurs at CG dinucleotides (mCG), here

we investigated both CG and non-CG contexts. Indeed, recent data has shown that non-CG methylation is not restricted to stem cells, and can be detected in brain tissue at even higher levels[11]. Available evidence also indicates that it progressively accumulates, preferentially in neurons, during the first decade of life[12, 13], a period when ELA typically occurs. Thus, we postulated that changes in non-CG methylation might contribute to life-long consequences of ELA, and focused in particular on the CAC context, where non-CG methylation is most abundant. Parallel analyses combining all epigenetic layers and transcriptomes converged to identify immune system processes and small GTPases as critical pathways associated with ELA, and suggested that ELA leaves distinct, albeit equally frequent, traces in CG and CAC sites. Altogether, our results suggest previously unforeseen sources of epigenetic and transcriptomic plasticity, which may likely contribute to the severe and lifelong impact of ELA on behavioural regulation, and the risk of psychopathology.

Results

Histone landscapes. Six histone modifications were assessed in subjects with histories of ELA (n=21) and healthy controls (C) with no such history (n=17; Supplementary Tables1,2). Following the International Human Epigenome Consortium (IHEC) procedures, we achieved >60 and >30 million reads for broad (H3K4me1, H3K36me3, H3K27me3 and H3K9me3) and narrow (H3K27ac and H3K4me3) marks, respectively (4.0 billion reads total; Fig.S1a, Supplementary Table3). Quality controls confirmed that all samples for the 2 narrow marks showed relative and normalized strand cross correlations that were, respectively, greater than 0.8 and 1.05 (Fig.S1b), according to expectations[14]. Read distribution within genes showed expected patterns (Fig.1a,b): reads were strongly enriched in Transcription Start Sites (TSS) regions for H3K27ac, H3K4me3 and H3K4me1, while H3K27me3 and H3K36me3 showed antagonistic distributions, consistent with results obtained in other tissues[10]. Samples strongly clustered by the type of mark, with a large distinction between activating and repressive marks (Fig.1c). To investigate tissue specificity of our dataset, we then compared it with data from other brain regions and blood tissue (from the NIH Roadmap Epigenomics; Fig.S2). For each modification, we observed higher correlations among amygdalar samples (r=0.75-0.92 across the 6 marks) than when compared with samples from other brain regions (r=0.51-0.81), and even lower correlations with peripheral blood mononuclear cells (r=0.35-0.64), consistent with the role of histones in tissue identity. We next investigated relationships between histone marks and gene expression (Fig.1d). As expected, we observed activating functions for H3K27ac, H3K4me1, H3K36me3 and H3K4me3, and repressive functions for H3K27me3 and H3K9me3. Distinct correlation profiles were observed between marks along the spectrum of gene expression levels, indicating that multiple marks are likely to better predict gene expression than individual ones. Comparisons between ELA and C groups found no significant overall

differences in terms of read distribution (Fig.1b) or relationship to gene expression (Fig.1d), indicating that ELA, as expected, does not globally reconfigure amygdalar histone landscapes.

Considering that different combinations of histone modifications define so-called chromatin states[15], we then conducted a combined analysis of all marks using ChromHMM machine-learning. Maps of chromatin states were generated as described previously[16], with each state corresponding to a distinct combination of individual marks. This unbiased approach defined a consensus map corresponding to genomic regions showing ≥70% agreement across samples (Fig.1e, and see *Methods*), and consistent with studies in the brain and other tissues[16-18]: for example, regions defined by a combination of H3K27ac and H3K4me1 corresponded to enhancers[19]. As detailed below, these maps allowed us to characterize cross-talks between chromatin states and DNA methylation, and differences between groups.

CG and non-CG methylation patterns. We used WGBS to characterize methylomes in both groups, generating a total of 6.2 billion reads. Rates of bisulfite conversion and over-conversion, sequencing depth, and library diversity met the IHEC standards and were similar across groups (Fig.S3a-d). In this large dataset, >13 million individual CGs showed an average coverage ≥5 in the entire cohort (Fig.S3e), which favourably compares with recent human brain studies in terms of sample size[20] or number of CGs covered[21, 22].

Because recent studies suggest that non-CG methylation is enriched in mammalian brains[11, 23], we first computed average genome-wide levels of methylation in multiple cytosine contexts. Focusing on 3-letter contexts (Fig.2a), we observed that, as expected, methylation levels were highly variable among the 16 possibilities (2-way ANOVA; context effect: [$F(15,540)=196283$; $p<0.0001$]), with much higher methylation levels in the CGA, CGC, CGG, and CGT contexts than in the 12 non-CG contexts. Of note, no difference was found in overall methylation between groups ([$F(1,36)=0.12$; $p=0.73$]), indicating, as expected, that ELA does not associate with a global dysregulation of the methylome. Among non-CG contexts, methylation was the highest at CACs (4.1±0.1%), followed by a group of contexts exhibiting between 1.8 to 1.1% average methylation (CTC, CAG, CAT, and CAA), while low levels (<0.4%) were observed for remaining contexts. This ordering was strikingly similar to what was recently described in the mouse brain[24] (Fig.S4a-b), suggesting a robust and conserved distribution of methylation according to sequence context. Considering that methylation at CA[25] or CAC[26] sites may have specific functions in the brain, and because CAC methylation (hereafter mCAC) was most abundant, we focused on this context in follow-up analyses.

We first compared the abundance of mCG and mCAC. While CG sites were highly methylated, CAC (Fig.2b-c) or other non-CG (Fig.S4c) sites were mostly unmethylated, with a minority of them showing methylation levels between 10 to 20%, consistent with mouse data[27]. Regarding distinct genomic features and chromosomal location, we confirmed that, while mCG

is lower within promoters (where CGs frequently cluster in CG islands), this effect is much less pronounced for mCAC (Fig.S5a)[11]. Further, we observed that (i) compared with CGs[28], depletion of methylation from pericentromeric regions is even stronger at CACs, and that (ii) methylation levels were extremely low in both contexts in the mitochondrial genome (Fig.S5b). We then confronted methylation data with measures of gene expression, regardless of group status, and found the expected anti-correlation in both contexts (Fig.2d; CG: [F(1,37)=557; p=6.7E-24]; CAC: [F(1,37)=3283; p=9.7E-38]). Because CAC sites, in contrast with CGs, are by definition asymmetric on the two DNA strands, we wondered whether this anti-correlation would be different when contrasting gene expression with mCAC levels on the gene's (sense) or the opposite (antisense) strand. No difference was found (Fig.S6), indicating that gene expression is predicted to the same extent by mCAC on either strand, at least for the coverage achieved here. These data emphasize noticeable differences and similarities between mCG and mCAC, and are consistent with results previously obtained for all non-CG contexts combined, in the mouse and in human[27, 29].

Regarding histone modifications, while mechanisms mediating their interactions with mCG have been documented[30], no data is currently available to describe such relationship for non-CG contexts. To address this gap, we confronted our consensus model of chromatin states (see Fig.1e) with DNA methylation. For both mCG ([F(1,36)=0.36; p=0.55]) and mCAC ([F(1,36)=0.07; p=0.80]; Fig.2e-f), genome-wide methylation levels were similar between groups across the 10 states, indicating that ELA does not associate with a global disruption of the cross-talk between DNA methylation and chromatin. Nevertheless, methylation levels strongly differed between states, in both CG ([F(9,324)=5127; p<0.0001]) and CAC ([F(9,324)=910.7; p<0.0001]) contexts, unravelling previously uncharacterized dissociations. First, in the CG context (Fig.2e) we observed a strong anti-correlation between DNA methylation and both forms of H3K4 methylation (me1, me3), consistent with findings in other cell types[30]: lowest mCG was observed in the 3 promoter states defined (Fig.1e) by high levels of H3K4me3 in combination with either high H3K4me1 (Flanking Promoter, Flk Prom; p<0.0001 for every post-hoc comparison, except against the Polycomb repressed state, PcR), high H3K27ac (Active Promoter, Act-Prom; p<0.0001 for every comparison against other states), or intermediate levels of both H3K27ac and H3K4me1 (Weak Promoter, Wk-Prom; p<0.0001 against other states). In contrast, among these 3 promoter states mCAC was particularly enriched in Wk-Prom regions (p<0.0001 against Act-Prom and Flk-Prom; Fig.2f). Second, mCG was abundant in transcribed regions defined by either intermediate H3K36me3 (Weak Transcription, Wk-Trans), or high H3K36me3 and low H3K27ac (Strong Transcription, Str-Trans). By contrast, mCAC was selectively decreased in the Str-Trans state (p<0.0001 against Wk-Trans). Third, while mCG levels were high in heterechromatin (Heteroch, defined by high H3K9me3 alone), consistent with its role in chromatin condensation, mCAC appeared

depleted from these regions ($p<0.0001$ for every comparison against other states, except PcR and Flk-Prom). Overall, results indicate that interactions between DNA methylation, histones, and chromatin strikingly differ across mCG and mCAC, possibly as a result of brain-specific epigenetic processes in the latter 3-letter context[29].

Changes in individual histone marks or chromatin states as a function of ELA. We investigated local adaptations in histone profiles of ELA subjects using diffReps[31]. A total of 5126 differential sites (DS) were identified across the 6 marks (Fig.3a-b, Fig.S7, Supplementary Table4) using consensus significance thresholds[32] ($p<10^{-4}$, FDR-$q<0.1$). Interestingly, H3K27ac contributed to 30% of all DS, suggesting a meaningful role of this mark in epigenetic changes associated with ELA. Annotation to genomic features revealed distinct distributions of DS across marks (df=25, χ^2 =1244, $p<0.001$; Fig.S8a): H3K4me1- and H3K4me3-DS were equally found in promoter regions and gene bodies, while H3K36me3- and H3K27ac-DS were highly gene-body enriched, and H3K27me3- and H3K9me3-DS found in intergenic/gene desert regions. Sites showing enrichment (up-DS) or depletion (down-DS) of reads in ELA subjects were found for each mark, with an increased proportion of down-DS associated with changes in H3K4me1, H3K4me3, H3K36me3 and H3K27me3 (Fig.S8b).

We then used GREAT (Supplementary Table5), a tool that maps regulatory elements to genes based on proximity, to test whether ELA subjects had perturbations in histone modifications that affected genes in specific pathways[33]. We performed this GO analysis for biological processes and molecular functions (Fig.3c-d) on each mark, and found significant enrichments for DS involving 3 marks: H3K27ac, H3K27me3 and H3K36me3. Importantly, overlaps between enriched GO terms were observed across marks: notably, terms related to immune processes, as well as small GTPases, were enriched for H3K36me3- and H3K27ac-DS, suggesting these pathways may play a significant role in ELA.

To strengthen these findings, a joint analysis of all marks was conducted using maps of chromatin state[15]. First, we identified genomic regions where a switch in chromatin state (state transitions, ST; n=61,922) occurred between groups (Supplementary Table6). Across the 90 possible ST in our 10-state ChromHMM model, only 56 were observed, with a high proportion (50.2%, indicated by * in Fig.4a) involving regions in quiescent (Quies), Wk-Trans or Enh states in the C group that mostly turned into Quies, Str-Trans, Wk-Trans, and Heteroch states in the ELA group. Furthermore, 17% and 59% of ST occurred in regions within 3kb of a promoter or in gene bodies (Fig.4b), respectively, suggesting that ELA-associated changes affected selected chromatin states, and mostly occurred within genes.

We next investigated GO enrichment of ST, using GREAT (Fig.4c-d, Supplementary Table7). As described previously[32], a co-occurrence score reflecting both the significance of GO terms and their recurrence across multiple STs was computed. Importantly, biological

processes (Fig.4c) with highest co-occurrence scores were similar to those found from the GO analysis of individual histone marks, and clustered in two main categories: immune system, and small GTPases. These terms were significant for state transitions involving transcription, quiescent and enhancer states. Regarding molecular functions (Fig.4d), most enriched gene categories were related to GTPases, and involved the same types of ST. Therefore, analyses at the level of individual histone marks and chromatin state converged to suggest global impairments in similar pathways.

Differential DNA methylation in ELA. We next sought to identify changes in DNA methylation. As the abundance of mCG and mCAC were very different, and considering data suggesting possible mCAC-specific processes[26], we used the BSmooth algorithm[34] to identify DMRs separately in each context, using strictly similar parameters (see *Methods*). DMRs were defined as regions of five or more clustered cytosines that each exhibited a significant difference in methylation ($p<0.001$), and an absolute methylation difference $\geq 1\%$ between groups. Surprisingly, we found that as many DMRs could be identified in the CAC context (n=866) as in the canonical CG context (n=878, Fig.5a-b). These 2 categories of DMRs were distributed throughout the genome and in every chromosome, while there was no direct overlap between genomic regions that they covered. Compared with CG-DMRs, CAC-DMRs were composed of slightly fewer cytosines (Fig.S10a, p=2.9E-04) and were smaller (Fig.S10b, p<2.2E-16). In addition, consistent with the overall lower abundance of mCAC, CG-DMRs affected sites showing a wide range of methylation levels, while CAC-DMRs were primarily located in lowly methylated regions (Fig.5c-d). Further, methylation changes detected in the ELA group were less pronounced in the CAC context, as shown by smaller percentage changes in methylation (p<2.2E-16; Fig.5e-f, Fig.S10c) and smaller areaStat values (the BSmooth measure of the statistical strength of methylation changes within DMRs[34]; p=5.8E-08, Fig.S10d). Overall, these results suggest that cytosines in the CAC context may represent a significant form of plasticity that may contribute to long-term consequences of ELA.

We next characterized genomic features where DMRs occurred, and observed that their distribution strikingly differed (p<2.2E-16; Fig.6a-b, Supplementary Table8): CG-DMRs were located in promoters (38.5% in proximal promoter, promoter1k and promoter3k) and gene bodies (35.4%), while CAC-DMRs were mostly found in gene bodies (53%) and intergenic regions (28.1%). Second, we characterized histone modifications around DMRs (Fig.6c-d, Fig.S11): CG-DMRs were enriched with H3K4me1, H3K4me3 and H3K27ac (Fig.6c), reinforcing our previous observations that these histone marks (Fig.1e) and DMRs (Fig.6a) were preferentially located in promoters. In sharp contrast, the 2 main features characterizing CAC-DMRs were an enrichment in H3K36me3 and a depletion in H3K9me3 (Fig.6d, Fig.S11). These differences were further supported by the analysis of chromatin states (p<2.2E-16;

Fig.6e, Fig.S12, Supplementary Table9). CAC-DMRs were largely absent from promoter (Act-Prom, Flk-Prom, and Wk-Prom) and enhancer (Str-Enh and Enh) states that were all defined, to varying degrees, by the 3 marks that primarily characterize CG-DMRs: H3K4me1, H3K4me3 and H3K27ac (Fig.1e). In addition, CAC-DMRs were (i) enriched in the Wk-Trans state, defined by the presence of H3K36me3, and (ii) depleted from the 2 states (PcR, Heteroch) characterized by the H3K9me3 mark. These effects were consistent with the enrichment and depletion previously observed individually for each of these 2 histone modifications, respectively.

Finally, we conducted a GREAT analysis of GO terms enriched for DMRs: CG-DMRs notably associated with terms related to the regulation of neuronal transmembrane potential (Fig.6f), in agreement with histone results (see Fig.4c), while CAC-DMRs were enriched for terms related to glial cells (glial cell differentiation; leukocyte migration, Fig.6g), consistent with the immune dysregulation previously observed with histone DS and ST. Altogether, while ELA associates with similar numbers of mCG and mCAC adaptations, these 2 types of plasticity occur in genomic regions characterized by different histone marks, chromatin states, and GO categories, possibly reflecting the implication of distinct molecular mechanisms.

Combining GO analyses. Analyses of histone modifications and DNA methylation identified GO terms consistently affected in ELA individuals. To determine how these epigenetic adaptations may ultimately modulate amygdalar function, we characterized gene expression in C and ELA groups, using RNA-Sequencing. Samples with similar RNA integrity across groups were sequenced at high depth (>50 million reads/sample), yielding good quality data (Fig.S13). Quantification of gene expression was conducted using HTSeq-count, as described previously[35], and validated by an alternative pseudo-alignment approach, Kallisto[36], generating very similar results ($r=0.82$, $p<2.2E-16$; Fig.S14a). A differential expression analysis between groups was then performed using DESeq2 (see full results in Supplementary Table10). Similar to our analyses of epigenetic datasets, we searched for patterns of global functional enrichment using GO and Gene Set Enrichment Analysis (GSEA)[35]. Enrichment of GO categories using the 735 genes that showed nominal differential expression in the ELA group ($p<0.05$, Fig.7a, Supplementary Table11) identified numerous terms consistent with our previous analyses at epigenetic level, including immune and small GTPase functions (Fig.7b). As a complementary approach, we used GSEA[37], which does not rely on an arbitrary threshold for significance, and takes directionality of gene expression changes into account. GSEA identified 163 genome-wide significant sets, among which 109 were related to immune processes and negatively correlated with ELA (Supplementary Table12, Fig.7c-d). Therefore, analysis of transcriptomic data identified gene pathways that in part overlap with those identified at the level of histone marks and DNA methylation.

To combine analyses conducted for histone modifications, chromatin states, DNA methylation and gene expression, we finally grouped GO terms enriched at each level to identify biological mechanisms most consistently affected (Fig.S14c). Overall, a clear pattern emerged whereby the highest number of genome-wide significant terms (n=122 GO terms) were related to immune processes, with contributions from each of the 4 types of data. Second came terms related to small GTPases, which were documented by histone modifications, chromatin states and gene expression (n=22), followed by terms related to neuronal physiology (n=19, mostly linked with neuronal excitability and sensory processing; Supplementary Table13), cellular adhesion (n=9), and the cytoskeleton (n=6). Overall, these combined analyses defined major epigenetic and transcriptomic pathways affected by ELA in the lateral amygdala.

Discussion

This study investigated 6 histone marks, DNA methylation and gene expression in, to our knowledge, one of the most comprehensive comparison of canonical mCG with the brain-enriched mCAC. In the healthy brain, striking differences in the relationship that the 2 forms of methylation exhibit with histone modifications were uncovered, providing avenues for mechanistic molecular studies. Also, going beyond previous studies of ELA[9], this work represents the first analysis of its consequences across multiple epigenetic layers. Results indicated that most extensive changes affect immune-related genes and small GTPases, in part through the reprogramming of chromatin and the methylome. Finally, results suggest that mCAC is plastic in the human brain, and may be developmentally regulated by ELA to a similar extent to what can be observed in the reference CG context, uncovering a potential new molecular substrate for the embedding of early-life experience.

We first integrated DNA methylation data with histone marks and gene expression to identify biological pathways most significantly associated with ELA in the lateral amygdala. Genome-wide analyses showed converging evidence for significant enrichment in immune-related GO terms (including genes encoding the complement system, Toll-like receptors, clusters of differentiation, the major histocompatibility complex), across all molecular layers, suggesting a meaningful contribution to psychopathological risk. Over the last two decades, considerable evidence has associated enhanced inflammation with stress-related phenotypes such as depression, in particular based on measures of cytokines and inflammatory factors in blood samples[38]. Limited molecular data, however, is available to understand how this pro-inflammatory state may translate at brain level, with few studies reporting inconsistent findings in cortical structures (with mostly increases but also decreases in the expression of inflammation-related genes[38]). Our findings therefore represent, to our knowledge, the first indication for altered immune processes in the lateral amygdala in relation to ELA and

associated depression. While the global pattern of downregulation we observed at gene expression level was surprising considering the general view that stress-related psychopathology associates with higher inflammation, it is nevertheless consistent with the lower density of glial cells described in the amygdala of depressed individuals (in some[39, 40] but not all[41] studies), which may notably concern microglial and astrocytic cells, the main immune actors in brain tissue.

The second pathway most significantly altered in ELA subjects was related to small GTPases, a large family of GTP hydrolases that among other processes regulate synaptic structural plasticity through interactions with the cytoskeleton[42]. Interestingly, the association observed for small GTPases was accompanied by significant changes affecting GO terms related to the cytoskeleton. Overall, this indicates that some form of synaptic plasticity occurs in the lateral amygdala as a function of ELA, and reveals part of the underlying epigenetic mechanisms. While very few molecular post-mortem studies support this hypothesis[43], it strongly resonates with the wealth of human imaging and animal data documenting structural and functional plasticity in this brain region as a function of stressful experiences[4].

We next used our extensive data set to conduct a detailed analysis of non-CG methylation. Over the last few years, the significance of this type of DNA methylation, and the possibility that it may fulfill biological functions, have been supported by several lines of evidence, including: (i) distinct methylation patterns shown to preferentially affect CAG sites in embryonic stem cells as opposed to CACs in neuronal and glial cells[11], (ii) the particular abundance of non-CG methylation in genes with a higher genomic size in the human brain[25], and (iii) the specific binding of the methyl-CpG-binding domain protein MeCP2 to both mCG and mCAC in the mouse brain[26, 44]. Here, we provide additional evidence reinforcing this notion, as we found that the relative frequency of non-CG methylation across 3-letter cytosine contexts is conserved in the human brain compared to mouse and, importantly, that mCAC exhibits peculiar interactions with the histone code as well as quantifiable plasticity in relation to ELA.

We first compared mCG and mCAC in distinct genomic features and chromatin states, regardless of clinical grouping. While interactions between DNA methylation and histone marks were described previously in other tissues[45, 46], and in the brain for mCG[45], here we unravel unforeseen specificities regarding mCAC. First, among the 3 chromatin promoter states (Act-Prom, Wk-Prom, Flk-Prom), mCAC was selectively enriched in Wk-Prom, which was not observed for mCG. Considering that Wk-Prom was relatively depleted in H3K27ac and H3K4me1 compared to the 2 other promoter states, it is possible to hypothesize that these 2 histone modifications may potentially repress mCAC accumulation in brain tissue. A second dissociation consisted in the fact that lower mCAC levels were measured in Str-Trans compared with Wk-Trans regions, while no such difference was observed in the CG context.

This may result at least in part from higher levels of H3K36me3 observed in the Str-Trans state. Third, among the 2 tightly compacted chromatin states defined by the repressive mark H3K9me3, PcR and Heteroch, the latter state was characterized by higher DNA methylation in the CG, but not in the CAC, context, as well as by a relative increase in H3K9me3 and a decrease in H3K27me3. While there is currently no data, to our knowledge, supporting a potential interaction between H3K27me3 and non-CG methylation[11], a role for H3K9me3 can be speculated considering studies of cellular reprogramming. Indeed, the *in vitro* dedifferentiation of fibroblasts into induced pluripotent stem cells associates with the restoration of non-CG methylation patterns characteristic of stem cells, except in genomic regions characterized by high levels of H3K9me3[47]. Therefore, the possibility exists that H3K9me3 may be implicated in the regulation of mCAC in the brain, an hypothesis that warrants further investigation.

Recently, a molecular pathway that may contribute to such differences among mCG and mCAC in the brain has started to be unravelled: the methyltransferase Dnmt3a was shown in the mouse to mediate progressive post-natal accumulation of DNA methylation in the CA context[13], while *in vivo* recruitment of MeCP2 was demonstrated to rely primarily on mCG and mCAC levels rather than by methylation at other contexts, including CAT, CAA, or CAG[26]. In combination with these rodent studies, our results therefore suggest that DNMT3a and MeCP2 may be implicated in the particular cross-talk that seem to emerge between mCAC and histone modifications during brain maturation, and suggest that future investigations should focus on their putative interaction with aforementioned specific marks (H3K27ac, H3K4me1, H3K36me3, and H3K9me3), and related histone-modifying enzymes.

Finally, we wondered whether mCAC might show some degree of plasticity in the human brain. We found that similar amounts of differential methylation events could be detected across CAC and CG contexts in ELA subjects, suggesting that mCAC might be sensitive to behavioral regulation. While previous studies clearly showed that ELA associates with widespread effects on mCG throughout the brain's genome, they were conducted using methodologies (methylated DNA immunoprecipitation coupled to microarrays[48], reduced representation bisulfite sequencing[35]) primarily designed for the investigation of mCG. In comparison, the present study using WGBS provides a more comprehensive and unbiased assessment of the overall methylome, and represents, to our knowledge, the first indication in humans that the brain-specific mCAC form of DNA methylation might be affected by ELA. This result is consistent with recent mouse work[49] that provided evidence for an effect of environmental enrichment, during the adolescence period, on non-CG methylation, suggesting that both positive and negative early-life experiences may have the capacity to modulate this non-canonical epigenetic mechanism. Importantly, our combined investigation of DNA methylation and histone marks provides further characterization of this form of plasticity.

Strikingly, mCAC and mCG changes occurred in genomic regions that appeared distinguishable at virtually any level of analysis, including genomic features, individual histone marks, chromatin states, and GO categories. Accordingly, CG-DMRs primarily located among promoter regions and gene bodies, were enriched in H3K4me1, H3K4me3 and H3K27ac, and were represented across all chromatin states. In comparison, CAC-DMRs were less frequently found in promoter, were enriched in H3K36me3 and depleted in H3K9me3, and mostly associated with 2 chromatin states, Quiescent and Wk Trans. Overall, these results suggest a model whereby the complex cascades of neurobiological adaptations associated with ELA may result from, or alternatively contribute to, distinct pathophysiological phenomenon that differentially manifest at the level of CG and CAC sites. It is also possible to speculate that part of these adaptations may result from the impact of ELA on mechanisms that drive the developmental emergence of mCAC. In the future, animal models will be instrumental in testing this hypothesis and in deciphering underlying molecular cross-talk among epigenetic layers.

In conclusion, the epigenetic and transcriptomic landscape of the lateral amygdala exhibit targeted reconfigurations as a function of ELA. This reprogramming can be detected consistently across multiple epigenetic layers, including the newly recognized form of DNA methylation affecting CAC sites. Future studies will hopefully define the extent to which non-CG methylation at CACs, and potentially at other cytosine contexts, contribute to adaptive and maladaptive encoding of life experiences in the brain.

Methods

Methods and any associated references are available in the online version of the paper.

Authors contributions

PEL and GT conceived the study. GGC, EM, JY and PEL performed RNA and DNA extractions. TK and TP provided library preparations and next-generation sequencing through the IHEC consortium, and AR prepared ChIP-Seq libraries. MAC and PEL analyzed histone data. ZA and PEL analyzed methylation data. JFT and PEL analyzed RNA-Seq data, while the Kallisto analysis was conducted by JCG. AP conducted the BSmooth differential methylation analysis. MA, LCV, CE, IY, NM and GT provided lab resources and equipment. PEL, MAC and GT prepared the manuscript, and all authors approved the final version of the manuscript.

Acknowledgments

PEL was supported by fellowships from the ‘Fondation Fyssen’, the Canadian Institutes of Health Research, the American Foundation for Suicide Prevention, the ‘Fondation pour la Recherche Médicale’, and by fundings from the Bettencourt-Schueller Foundation, the Brain Canada Foundation, the ‘Fondation Deniker’, the ‘Congrès Français de Psychiatrie’, the ‘Fondation de France’ (N°Engt:00081244) and the ‘Union Nationale de Familles et Amis de Personnes Malades et/ou Handicapées Psychiques’.

Figure1

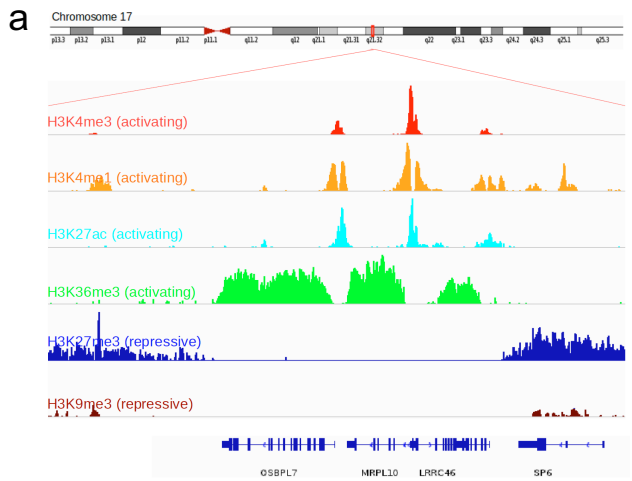
a
Chromosome 17
H3K4me3 (activating)
H3K4me1 (activating)
H3K27ac (activating)
H3K36me3 (activating)
H3K27me3 (repressive)
H3K9me3 (repressive)
OSBPL7
MRPL10
LRRC46
SP6

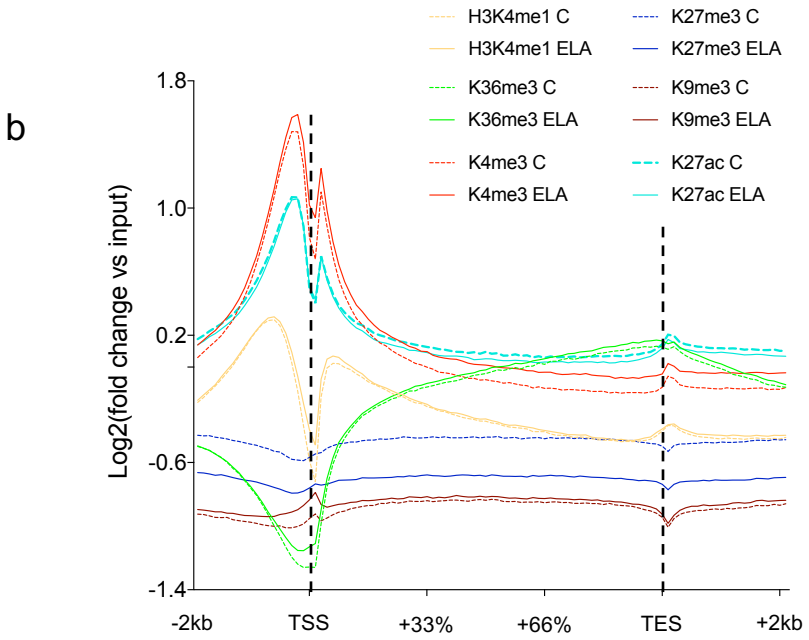
b
H3K4me1 C
H3K4me1 ELA
K36me3 C
K36me3 ELA
K4me3 C
K4me3 ELA
K27me3 C
K27me3 ELA
K9me3 C
K9me3 ELA
K27ac C
K27ac ELA
Log2(fold change vs input)
1.8
1.0
0.2
-0.6
-1.4
-2kb
TSS
+33%
+66%
TES
+2kb

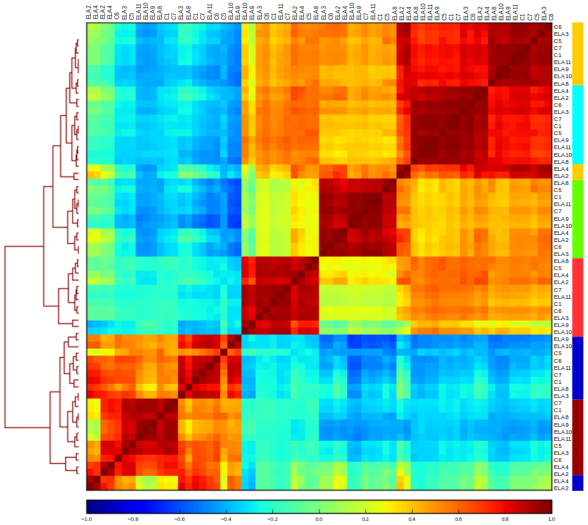
c

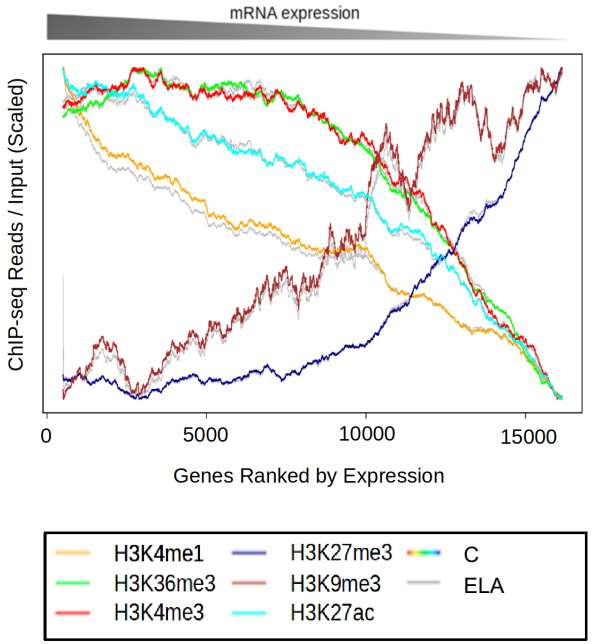
d
mRNA expression
ChIP-seq Reads / Input (Scaled)
0
5000
10000
15000
Genes Ranked by Expression
H3K4me1
H3K36me3
H3K4me3
H3K27me3
H3K9me3
H3K27ac
C
ELA

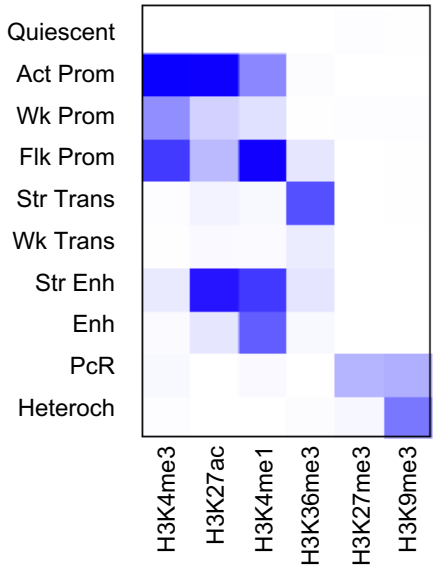
e
Quiescent
Act Prom
Wk Prom
Flk Prom
Str Trans
Wk Trans
Str Enh
Enh
PcR
Heteroch
H3K4me3
H3K27ac
H3K4me1
H3K36me3
H3K27me3
H3K9me3

Figure 1. Characterization of 6 histone post-translational modifications in the human brain lateral amygdala. (a) Snapshots of typical ChIP-seq read distribution for the six histone marks. **(b)** Average enrichment over input of ChIP-seq reads across all gene bodies and their flanking regions (+/- 2 kilobases, kb) in the human genome, for each histone mark. Note the expected biphasic distribution of reads around the Transcription Start Site (TSS) for H3K27ac, H3K4me3 and H3K4me1. No significant differences were observed for any mark across C and ELA groups (2-way Repeated Measures ANOVA, group effects: H3K4me1, p=0.89; H3K36me3, p=0.87; H3K4me3, p=0.64; H3K27me3, p=0.35; H3K9me3, p=0.88; H3K27ac, p=0.86). Averages for the healthy controls group (C) are shown as dashed lines, while averages for the early-life adversity group (ELA) are shown as solid lines. TES, Transcription End Site. **(c)** Unsupervised hierarchical clustering using Pearson correlations for all marks. Correlations were computed using read number per 10 kb-bins across the whole genome, and normalized to input and library size. Note the expected separation between activating (H3K27ac, H3K36me3, H3K4me1, H3K4me3) and repressive (H3K27me3, H3K9me3) marks. **(d)** Average enrichment of reads over gene bodies (for H3K27me3, H3K36me3, H3K4me1 and H3K9me3) or TSS +/- 1kb (for H3K27ac and H3K4me3) for all genes ranked from most highly (left) to least (right) expressed. Strongly significant effects of gene ranking on ChIP-Seq reads were observed for all marks ($p<0.0001$). Again, no difference was observed as a function of ELA for any group (2-way Repeated Measures ANOVA, group effects: H3K4me1, p=0.66; H3K36me3, p=0.67; H3K4me3, p=0.98; H3K27me3, p=0.31; H3K9me3, p=0.74; H3K27ac, p=0.48). **(e)** ChromHMM emission parameters (see main text and *Methods*) for the 10-state model of chromatin generated using data from the 6 histone marks, at a resolution of 200bp, as described previously[16]. Maps of chromatin states have already been characterized in other brain regions (e.g. cingulate cortex, caudate nucleus, substantia nigra[45]) but, to our knowledge, not in the amygdala. Chromatin states: Act-Prom, active promoter; Wk-Prom, weak promoter; Flk-Prom, flanking promoter; Str-Trans, strong transcription; Wk-Trans, weak transcription; Str-Enh, strong enhancer; Enh, enhancer; PcR, polycomb repressed; Heterochr, heterochromatin.

Figure2

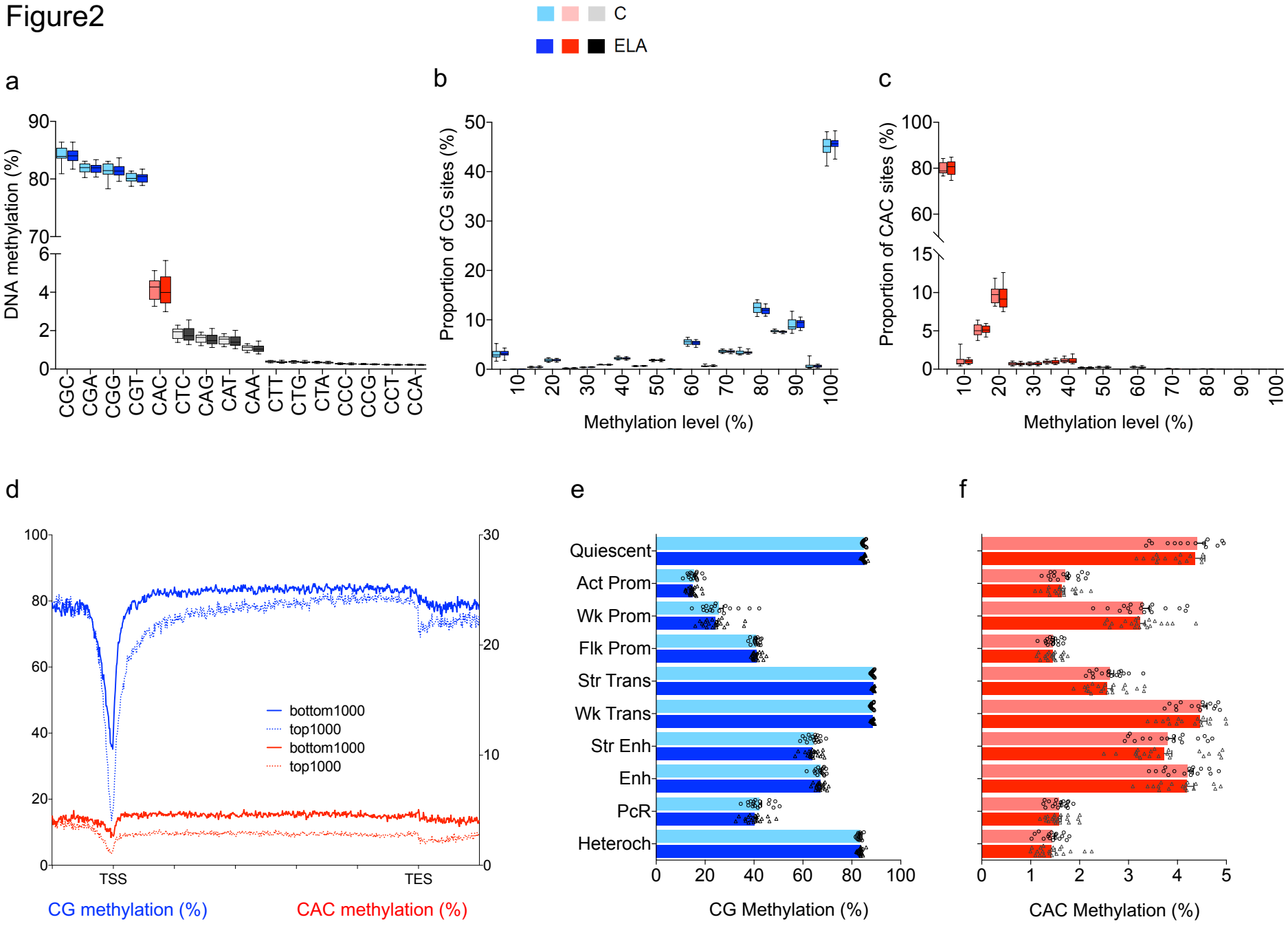
C
ELA
a
DNA methylation (%)
CGC
CGA
CGG
CGT
CAC
CTC
CAG
CAT
CAA
CTT
CTG
CTA
CCC
CCG
CCT
CCA
b
Proportion of CG sites (%)
Methylation level (%)
c
Proportion of CAC sites (%)
Methylation level (%)
d
bottom1000
top1000
bottom1000
top1000
TSS
TES
CG methylation (%)
CAC methylation (%)
e
Quiescent
Act Prom
Wk Prom
Flk Prom
Str Trans
Wk Trans
Str Enh
Enh
PcR
Heteroch
CG Methylation (%)
f
CAC Methylation (%)

Figure 2. Characterization of non-CG methylation in the human brain lateral amygdala. **(a)** Average genome-wide levels of DNA methylation were measured among the sixteen 3-letter cytosine contexts (CHH, where H stands for A, C, and T) in the human brain lateral amygdala, using whole-genome bisulfite sequencing. While highest DNA methylation levels were observed in the 4 CGN contexts (where N stands for any base; CGC: 84.1±0.2%; CGA: 81.9±0.1%; CGC: 81.4±0.2%, CGT: 80.2±0.1%; mean±sem in the whole cohort), detectable non-CG methylation was also observed in CHN context, most notably at CAC sites (4.1±0.1% in combined control, C, and early-life adversity, ELA, groups), with no detectable differences between groups for any context (2-way Repeated Measures ANOVA; group effect: [F(1,36)=0.12; p=0.73]). **(b)** DNA methylation in the CG context mostly corresponded to sites highly methylated. In contrast, as previously described in the mouse hippocampus[27], most CAC sites were unmethylated **(c)**, with only a minority of sites showing low methylation levels, between 10 and 20%. This likely reflects the fact that non-CG methylation does not occur in all cell types, and is notably enriched in neuronal cells and, to a lesser extent, in glial cells[11]. In the CG or CAC contexts (2-way ANOVA; group effect: CG, [F(1,720)=5.0E-11; p>0.99]; CAC, [F(1,36)=0; p>0.99]), ELA did not associate with any significant change in these global distributions. Box plots show median and interquartile range, with whiskers representing minimum and maximum values. **(d)** In both contexts, patterns of DNA methylation along gene bodies showed the expected anti-correlation with gene expression, as shown here comparing the 1000 most highly (top1000) or lowly (bottom1000) expressed genes, consistent with previous rodent data. TSS, Transcription Start Site; TES, Transcription End Site. In the CG **(e)** or CAC **(f)** contexts, no difference in DNA methylation levels was observed between C and ELA groups for any chromatin state. We observed, however, dissociations in the relationship of DNA methylation and histone marks across the CG and CAC contexts (see main text). Values are mean±sem. Chromatin states: Act-Prom, active promoter; Wk-Prom, weak promoter; Flk-Prom, flanking promoter; Str-Trans, strong transcription; Wk-Trans, weak transcription; Str-Enh, strong enhancer; Enh, enhancer; PcR, polycomb repressed; Heterochr, heterochromatin.

Figure3

a

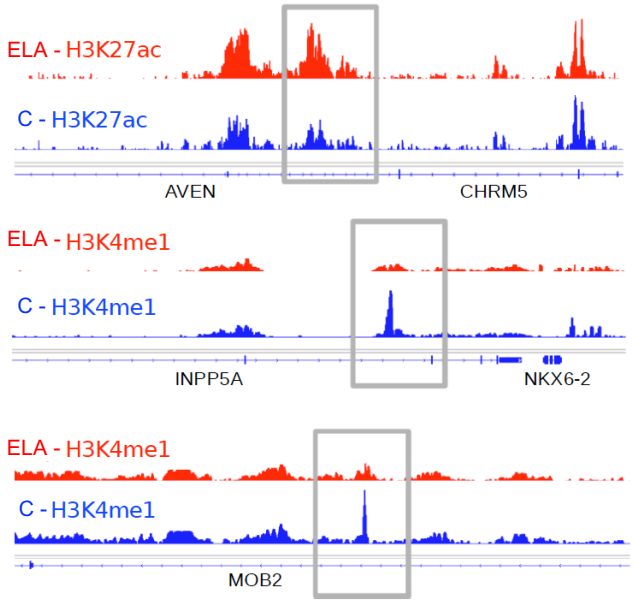

b

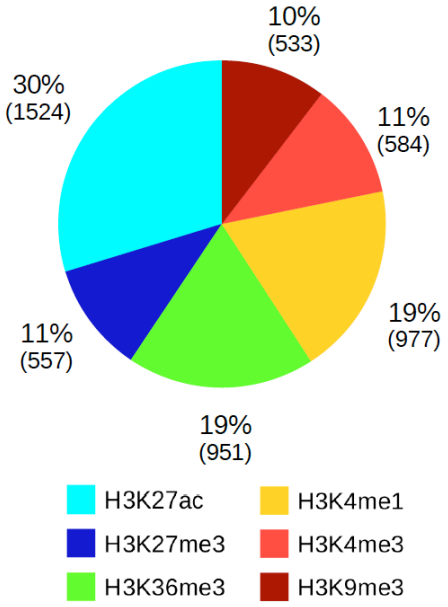

c

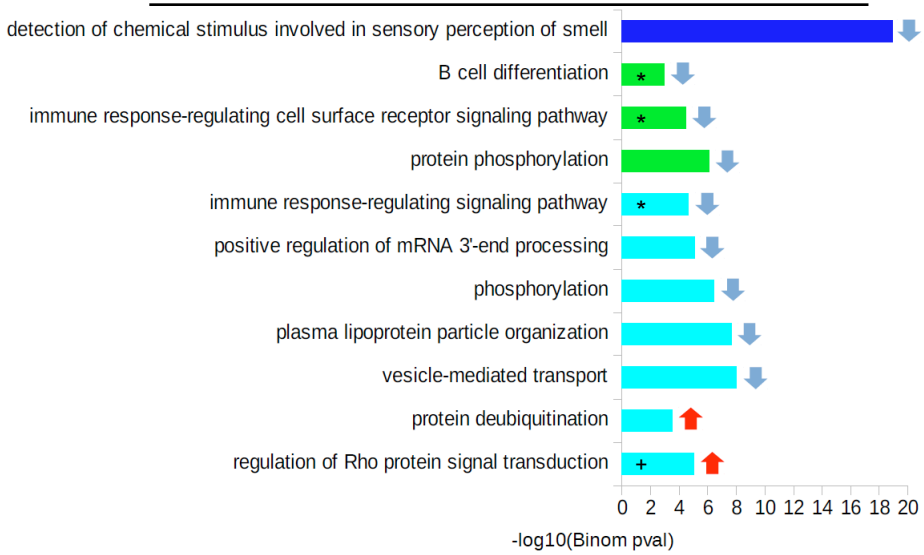

d

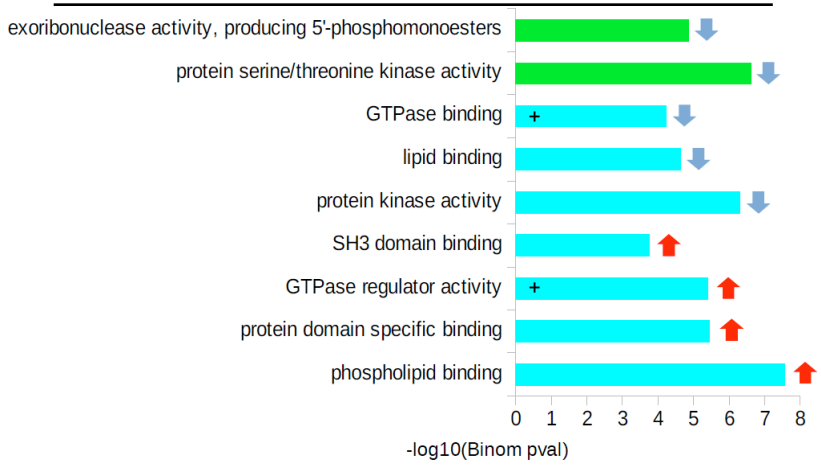

Figure 3. Analysis of genomic sites showing differential enrichment for individual histone marks in subjects with a history of early-life adversity (ELA). (a) Representation of three top Differential Sites (DS), identified using diffReps[31]. ELA are shown in red, healthy controls (C) are shown in blue. Grey rectangles delineate the coordinates of each DS. **(b)** Relative proportion of DS contributed by each histone mark. Percentages of total number of DS, and absolute number of DS (in brackets) are shown for each mark. Both depletion- and enrichment-DS were observed for each of the 6 marks (Fig.S8b). Among genes most strongly affected (Supplementary Table6), several have been previously associated with psychopathology, such as QKI (H3K27ac top hit)[35, 50] or HTR1A (H3K4me3 top hit)[51]. **(c-d)** Top five most significant non-redundant gene ontology "Biological Processes" **(c)** or "Molecular Functions" **(d)** terms enriched for each histone mark DS, as identified by GREAT[33] using hypergeometric and binomial testing (fold change≥1.5 and FDR-q≤0.1 for both tests). Surprisingly, the single most significant result implicated epigenetic dysregulation of odor perception in ELA subjects (consistent with recent clinical studies[52]), while immune processes (indicated by *), and small GTPases (+) were consistently found affected across different marks. Negative logarithmic p-values are shown for binomial testing. Color indicates histone mark concerned, arrows indicate direction of event: terms associated with depletion- (down arrow) or enrichment-DS (up arrow).

Figure4

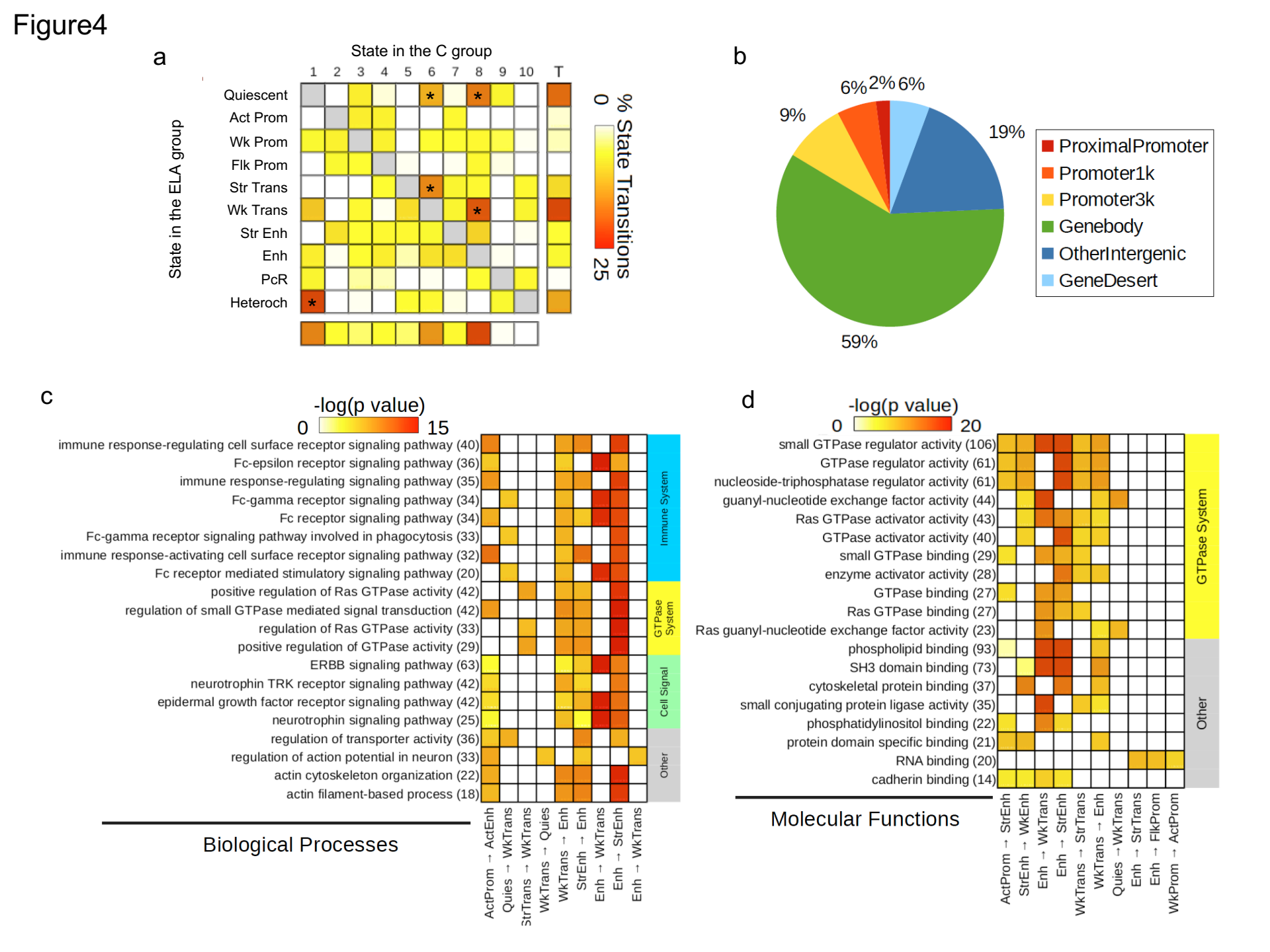
a
State in the C group
1 2 3 4 5 6 7 8 9 10 T
State in the ELA group
Quiescent
Act Prom
Wk Prom
Flk Prom
Str Trans
Wk Trans
Str Enh
Enh
PcR
Heteroch
% State Transitions
0
25
b
6%
2%
6%
9%
19%
59%
ProximalPromoter
Promoter1k
Promoter3k
Genebody
OtherIntergenic
GeneDesert
c
-log(p value)
0
15
immune response-regulating cell surface receptor signaling pathway (40)
Fc-epsilon receptor signaling pathway (36)
immune response-regulating signaling pathway (35)
Fc-gamma receptor signaling pathway (34)
Fc receptor signaling pathway (34)
Fc-gamma receptor signaling pathway involved in phagocytosis (33)
immune response-activating cell surface receptor signaling pathway (32)
Fc receptor mediated stimulatory signaling pathway (20)
positive regulation of Ras GTPase activity (42)
regulation of small GTPase mediated signal transduction (42)
regulation of Ras GTPase activity (33)
positive regulation of GTPase activity (29)
ERBB signaling pathway (63)
neurotrophin TRK receptor signaling pathway (42)
epidermal growth factor receptor signaling pathway (42)
neurotrophin signaling pathway (25)
regulation of transporter activity (36)
regulation of action potential in neuron (33)
actin cytoskeleton organization (22)
actin filament-based process (18)
Immune System
GTPase System
Cell Signal
Other
ActProm → ActEnh
Quies → WkTrans
StrTrans → WkTrans
WkTrans → Quies
WkTrans → Enh
StrEnh → Enh
Enh → WkTrans
Enh → StrEnh
Enh → WkTrans
Biological Processes
d
-log(p value)
0
20
small GTPase regulator activity (106)
GTPase regulator activity (61)
nucleoside-triphosphatase regulator activity (61)
guanyl-nucleotide exchange factor activity (44)
Ras GTPase activator activity (43)
GTPase activator activity (40)
small GTPase binding (29)
enzyme activator activity (28)
GTPase binding (27)
Ras GTPase binding (27)
Ras guanyl-nucleotide exchange factor activity (23)
phospholipid binding (93)
SH3 domain binding (73)
cytoskeletal protein binding (37)
small conjugating protein ligase activity (35)
phosphatidylinositol binding (22)
protein domain specific binding (21)
RNA binding (20)
cadherin binding (14)
GTPase System
Other
ActProm → StrEnh
StrEnh → WkEnh
Enh → WkTrans
Enh → StrEnh
WkTrans → StrTrans
WkTrans → Enh
Quies → WkTrans
Enh → StrTrans
Enh → FlkProm
WkProm → ActProm
Molecular Functions

Figure 4. Analysis of genomic sites showing a switch between chromatin states as a function of early-life adversity (ELA). (a) Percentage of each State Transition (ST) type relative to the total number of transitions. For the healthy control (C) versus ELA group comparison, the cumulative percentages of ST from a specific state to any other state are shown in the "Total" and "T" rows/columns. * indicates most frequent STs (see main text). **(b)** Distribution of ST localizations relative to genomic features, assessed using region_analysis[31] (see *Methods*; pericentromeric and subtelomeric categories not shown). **(c-d)** Gene ontology "Biological Processes" **(c)** or "Molecular Functions" **(d)** terms significantly associated with at least three types of ST. Terms are grouped based on overall system involved, and ranked by co-occurrence score (in parentheses after each term), which reflects both the significance of GO terms and their recurrence across multiple ST (see main text and[32]). Individual binomial p-values for each type of ST and each term are shown by color gradient. Each term also passed hypergeometric testing. Immune-related and small GTPase terms were most strongly affected, across multiple ST. Of note, a complementary GREAT pathway analysis using MSigDB further strengthened these findings by revealing recurrent enrichment (across six types of ST, as well as for H3K27ac down-DS; see Fig.S9) of the integrin signalling pathway, which is known to interact extensively with small GTPases[53].

Figure5

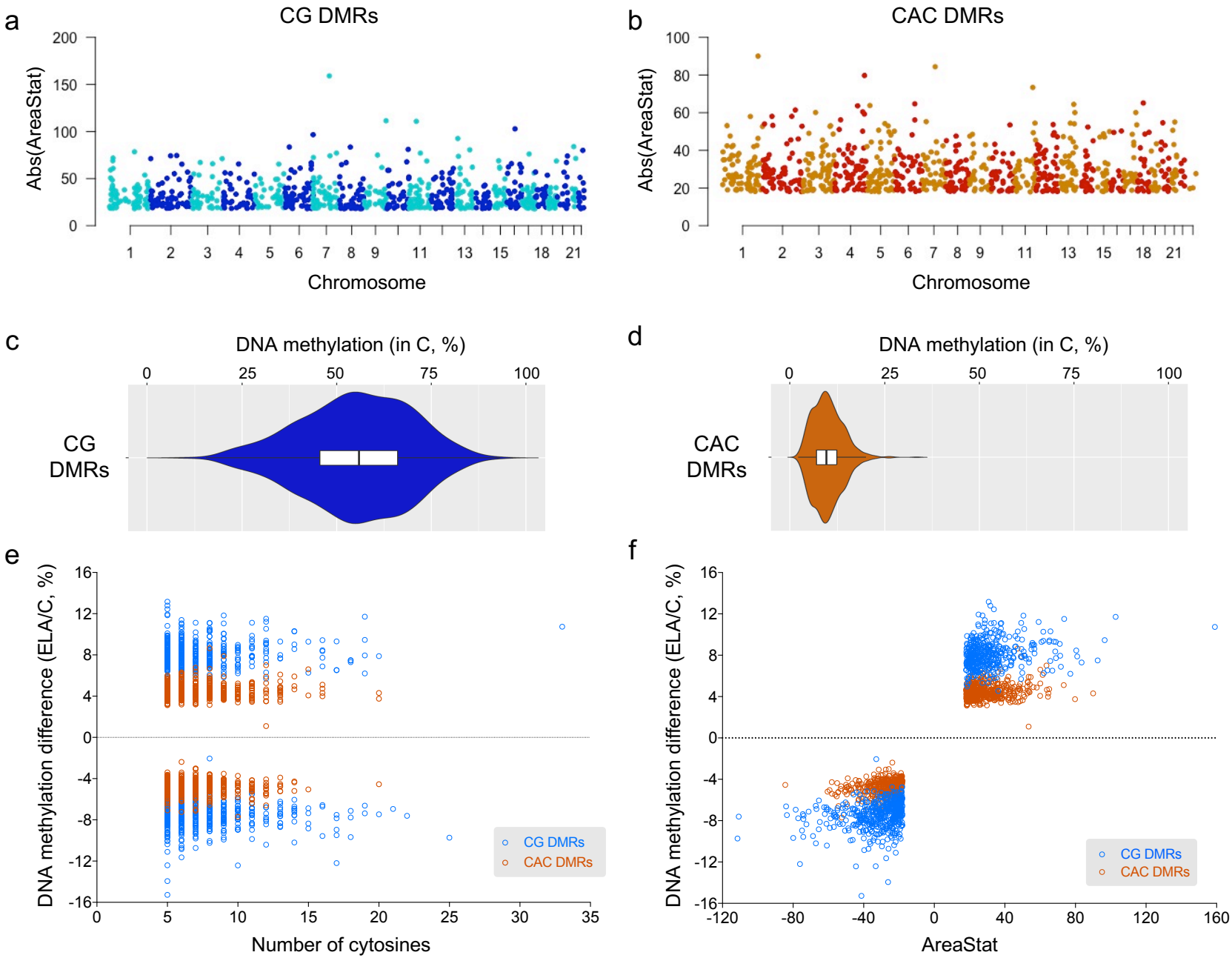
a
CG DMRs
Abs(AreaStat)
Chromosome
b
CAC DMRs
Abs(AreaStat)
Chromosome
c
DNA methylation (in C, %)
CG DMRs
d
DNA methylation (in C, %)
CAC DMRs
e
DNA methylation difference (ELA/C, %)
Number of cytosines
CG DMRs
CAC DMRs
f
DNA methylation difference (ELA/C, %)
AreaStat
CG DMRs
CAC DMRs

Figure 5. Differential DNA methylation in the CG and CAC contexts in subjects with a history of early-life adversity (ELA). (a-b) Manhattan plots of differentially methylated regions (DMR) identified using the BSmooth algorithm in the CG and CAC contexts, comparing control (C) and ELA groups. DMRs were identified separately in each context using the BSmooth algorithm[34], with strictly similar parameters (see *Methods*). They were defined as regions of ≥5 clustered cytosines that each exhibited a significant difference in methylation ($p<0.001$) and an absolute methylation difference ≥1% between groups. Surprisingly, as many DMRs were identified in the CAC context (n=866) as in the canonical CG context (n=878). **(c-d)** Methylation abundance in the C group in regions where DMRs were identified in the CG and CAC contexts. CG-DMRs affected genomic sites showing a wide range of methylation levels (mean±sem=55.3±0.5%), while CAC-DMRs occurred in lowly methylated regions (mean±sem=10.0±0.1%), resulting in significantly different distributions (Mann-Whitney U=686; $p<0.0001$). Box plots show median and interquartile range (IQR), with whiskers representing 1.5 × IQR. **(e)** DNA methylation differences observed in ELA subjects compared to the C group in CG and CAC DMRs, as a function of the number of cytosines composing each DMR. **(f)** DNA methylation differences observed in ELA subjects compared to the C group in CG- and CAC-DMRs, as a function of areaStat values, a measure of the statistical significance of each DMR implemented by BSmooth.

Figure6

a

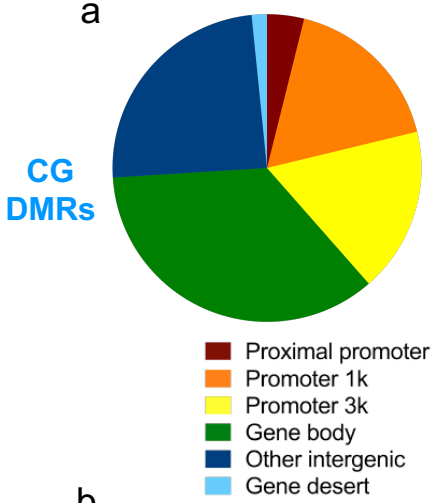

b

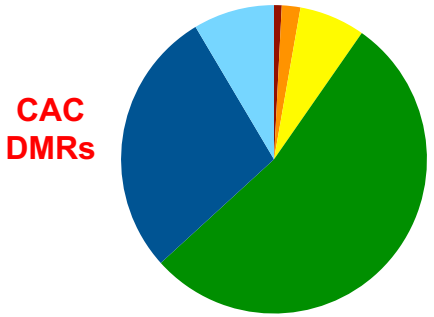

c

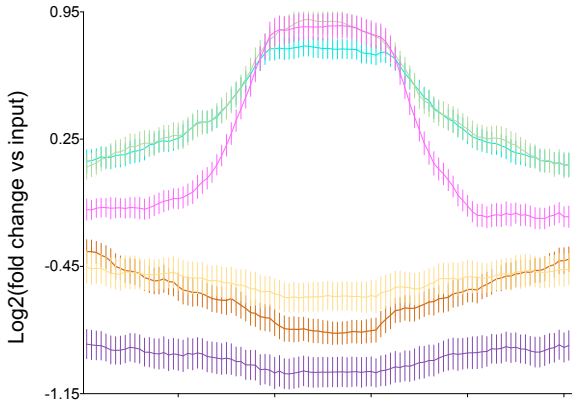

d

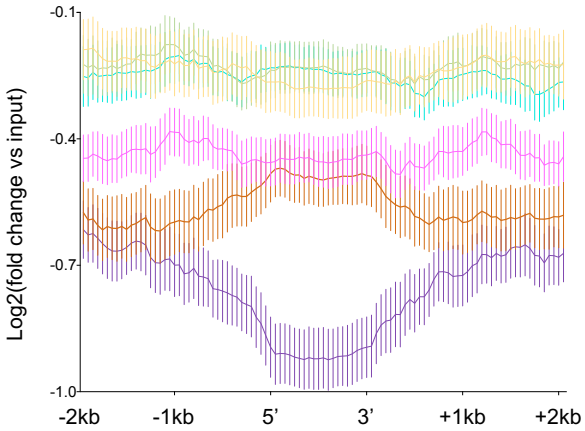

e

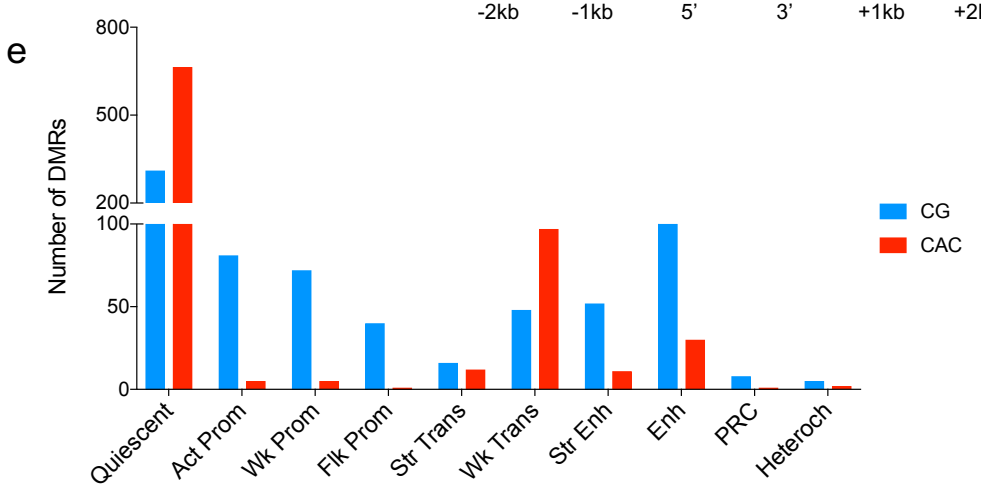

f

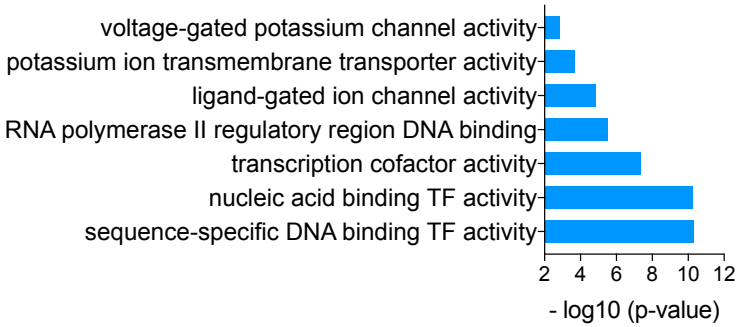

g

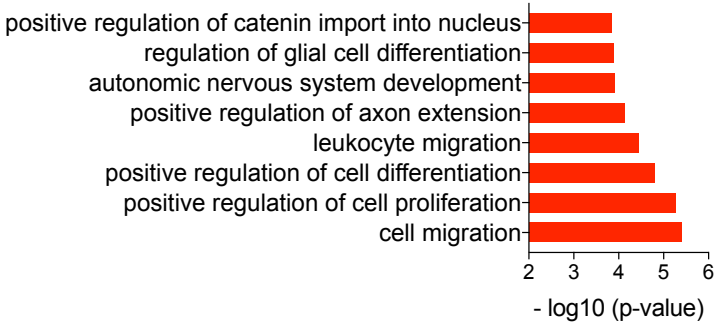

Figure 6. Individual histone marks and global chromatin states defining genomic regions where early-life adversity (ELA) associated with differential DNA methylation. **(a-b)** Localization of differentially methylated regions (DMR) in genomic features, identified using region_analysis[31]. Distributions were strongly different among CG and CAC contexts (χ^2=221.2, df=6, p<2.2E-16). **(c-d)** Histone modifications measured at the level of DMRs and their flanking regions (+/- 2 kilobases, kb). Distributions were very distinct between CG- and CAC-DMRs, with significant interactions between cytosine context and cytosine position along DMRs, for each of the 6 marks (2-way Repeated Measures ANOVA interactions, p<0.0001 for all; see also Fig.S11). Values are mean±sem. **(e)** Chromatin states found at DMRs. Similarly, CG- and CAC-DMRs occurred in very different chromatin states (χ^2=390.4, df=9, p<2.2E-16). **(f-g)** Gene Ontology analysis of CG and CAC DMRs using GREAT[33] (see main text).

Figure7

a

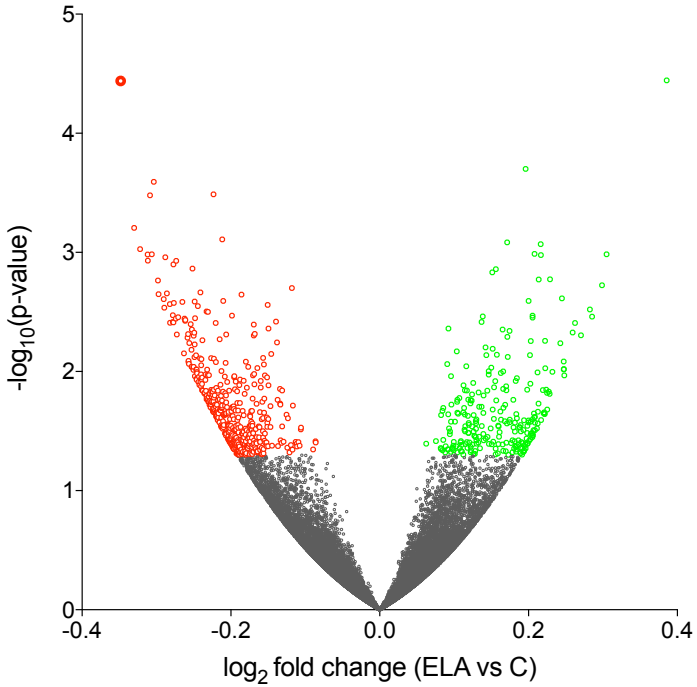

b

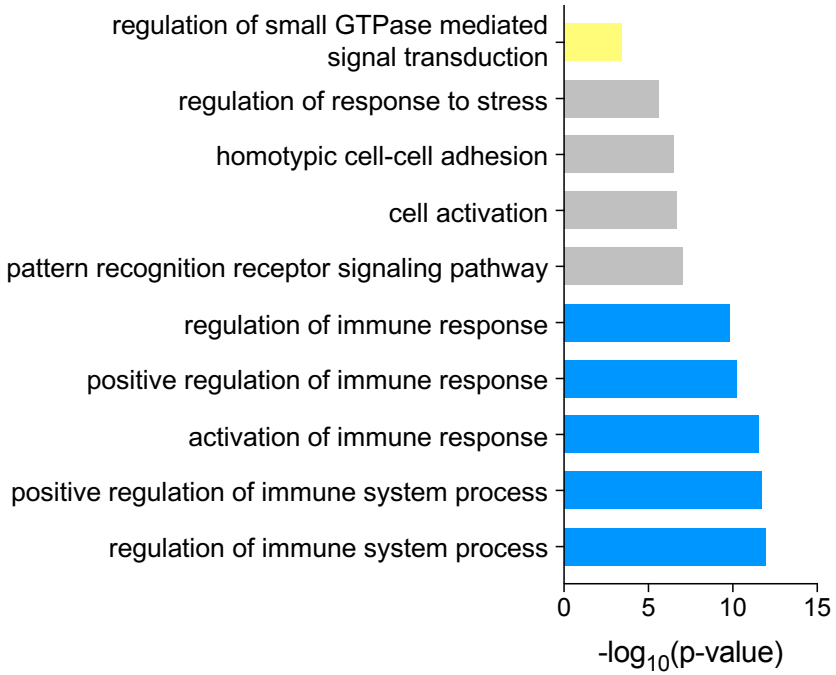

c

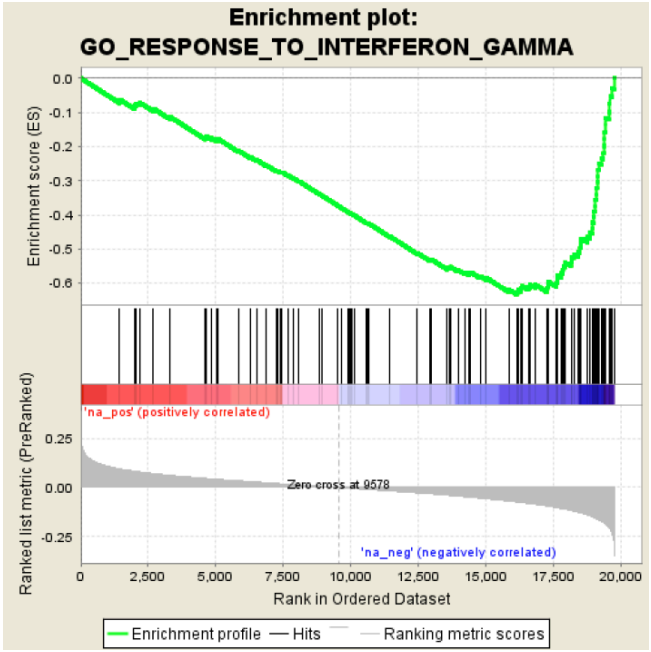

d

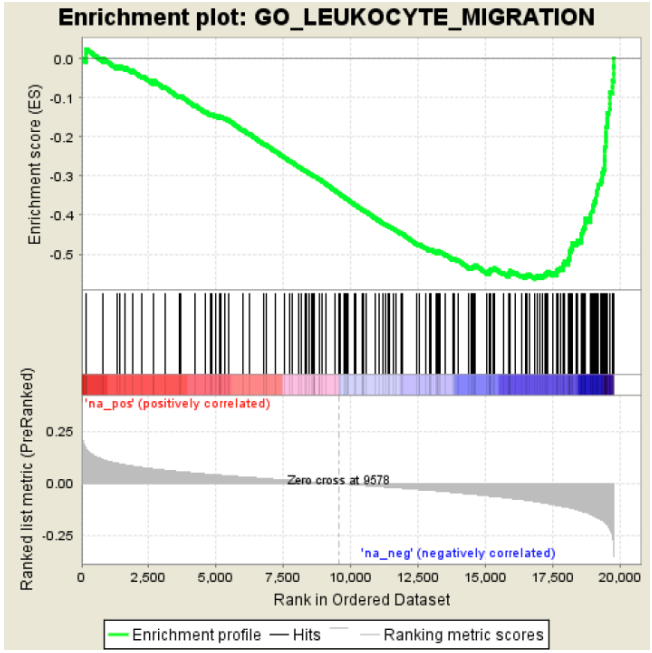

Figure 7. Differential gene expression in subjects with a history of early-life adversity (ELA). (a) Volcano Plot of RNA-Seq data showing the 261 and 474 genes that were up- (green circles) or down- (red circles) regulated in the ELA group compared with the control (C) group (nominal p-value<0.05). **(b)** Gene Ontology analysis of the 735 differentially expressed genes in the ELA group. **(c-d)** Gene Set Enrichment Analysis (GSEA) of gene expression changes in ELA subjects. Among the numerous gene sets related to immune function that showed evidence of genome-wide significant negative correlation with ELA (see main text, Supplementary Table12 and Fig.7c-d), 2 representative examples are shown here: 'Interferon gamma' and 'Leukocyte migration'. Of note, an analysis using c2 gene sets (from MSigDB; see Fig.S14b) indicated that an oligodendrocyte-specific gene collection, which we recently found downregulated in the cingulate cortex of subjects with a history of ELA[35], positively correlated with ELA in the amygdala, suggesting opposite adaptations in this glial population between cortical and subcortical structures.

References

1. Gilbert, R.*, et al.* Burden and consequences of child maltreatment in high-income countries. *Lancet* **373**, 68-81 (2009).
2. Nemeroff, C.B. Paradise Lost: The Neurobiological and Clinical Consequences of Child Abuse and Neglect. *Neuron* **89**, 892-909 (2016).
3. Teicher, M.H., Samson, J.A., Anderson, C.M. & Ohashi, K. The effects of childhood maltreatment on brain structure, function and connectivity. *Nat Rev Neurosci* **17**, 652-666 (2016).
4. Janak, P.H. & Tye, K.M. From circuits to behaviour in the amygdala. *Nature* **517**, 284-292 (2015).
5. Padival, M.A., Blume, S.R., Vantrease, J.E. & Rosenkranz, J.A. Qualitatively different effect of repeated stress during adolescence on principal neuron morphology across lateral and basal nuclei of the rat amygdala. *Neuroscience* **291**, 128-145 (2015).
6. Tsai, S.F.*, et al.* Social instability stress differentially affects amygdalar neuron adaptations and memory performance in adolescent and adult rats. *Front Behav Neurosci* **8**, 27 (2014).
7. Nagy, C. & Turecki, G. Sensitive periods in epigenetics: bringing us closer to complex behavioral phenotypes. *Epigenomics* **4**, 445-457 (2012).
8. Cole, P.M., Michel, M.K. & Teti, L.O. The development of emotion regulation and dysregulation: a clinical perspective. *Monogr Soc Res Child Dev* **59**, 73-100 (1994).
9. Burns, S.B., Szyszkowicz, J.K., Luheshi, G.N., Lutz, P.E. & Turecki, G. Plasticity of the epigenome during early-life stress. *Semin Cell Dev Biol* (2017).
10. Barski, A.*, et al.* High-resolution profiling of histone methylations in the human genome. *Cell* **129**, 823-837 (2007).
11. He, Y. & Ecker, J.R. Non-CG Methylation in the Human Genome. *Annu Rev Genomics Hum Genet* **16**, 55-77 (2015).
12. Lister, R.*, et al.* Global epigenomic reconfiguration during mammalian brain development. *Science* **341**, 1237905 (2013).
13. Stroud, H.*, et al.* Early-Life Gene Expression in Neurons Modulates Lasting Epigenetic States. *Cell* (2017).
14. Landt, S.G.*, et al.* ChIP-seq guidelines and practices of the ENCODE and modENCODE consortia. *Genome Res* **22**, 1813-1831 (2012).
15. Ernst, J. & Kellis, M. Chromatin-state discovery and genome annotation with ChromHMM. *Nat Protoc* **12**, 2478-2492 (2017).
16. De Jager, P.L.*, et al.* Alzheimer's disease: early alterations in brain DNA methylation at ANK1, BIN1, RHBDF2 and other loci. *Nat Neurosci* **17**, 1156-1163 (2014).

17. Day, K.*, et al.* Differential DNA methylation with age displays both common and dynamic features across human tissues that are influenced by CpG landscape. *Genome Biol* **14**, R102 (2013).
18. Sun, D. & Yi, S.V. Impacts of Chromatin States and Long-Range Genomic Segments on Aging and DNA Methylation. *PLoS One* **10**, e0128517 (2015).
19. Creyghton, M.P.*, et al.* Histone H3K27ac separates active from poised enhancers and predicts developmental state. *Proc Natl Acad Sci U S A* **107**, 21931-21936 (2010).
20. Sanchez-Mut, J.V.*, et al.* Human DNA methylomes of neurodegenerative diseases show common epigenomic patterns. *Transl Psychiatry* **6**, e718 (2016).
21. Jaffe, A.E.*, et al.* Mapping DNA methylation across development, genotype and schizophrenia in the human frontal cortex. *Nat Neurosci* **19**, 40-47 (2016).
22. Nagy, C.*, et al.* Astrocytic abnormalities and global DNA methylation patterns in depression and suicide. *Mol Psychiatry* (2014).
23. Schultz, M.D.*, et al.* Human body epigenome maps reveal noncanonical DNA methylation variation. *Nature* (2015).
24. Mo, A.*, et al.* Epigenomic Signatures of Neuronal Diversity in the Mammalian Brain. *Neuron* **86**, 1369-1384 (2015).
25. Gabel, H.W.*, et al.* Disruption of DNA-methylation-dependent long gene repression in Rett syndrome. *Nature* **522**, 89-93 (2015).
26. Lagger, S.*, et al.* MeCP2 recognizes cytosine methylated tri-nucleotide and di-nucleotide sequences to tune transcription in the mammalian brain. *PLoS Genet* **13**, e1006793 (2017).
27. Guo, J.U.*, et al.* Distribution, recognition and regulation of non-CpG methylation in the adult mammalian brain. *Nat Neurosci* (2013).
28. Luo, C.*, et al.* Cerebral Organoids Recapitulate Epigenomic Signatures of the Human Fetal Brain. *Cell Rep* **17**, 3369-3384 (2016).
29. Lee, J.H., Park, S.J. & Nakai, K. Differential landscape of non-CpG methylation in embryonic stem cells and neurons caused by DNMT3s. *Sci Rep* **7**, 11295 (2017).
30. Cedar, H. & Bergman, Y. Linking DNA methylation and histone modification: patterns and paradigms. *Nat Rev Genet* **10**, 295-304 (2009).
31. Shen, L.*, et al.* diffReps: detecting differential chromatin modification sites from ChIP-seq data with biological replicates. *PLoS One* **8**, e65598 (2013).
32. Feng, J.*, et al.* Chronic cocaine-regulated epigenomic changes in mouse nucleus accumbens. *Genome Biol* **15**, R65 (2014).
33. McLean, C.Y.*, et al.* GREAT improves functional interpretation of cis-regulatory regions. *Nat Biotechnol* **28**, 495-501 (2010).

34. Hansen, K.D., Langmead, B. & Irizarry, R.A. BSmooth: from whole genome bisulfite sequencing reads to differentially methylated regions. *Genome Biol* **13**, R83 (2012).
35. Lutz, P.E.*, et al.* Association of a History of Child Abuse With Impaired Myelination in the Anterior Cingulate Cortex: Convergent Epigenetic, Transcriptional, and Morphological Evidence. *Am J Psychiatry* **174**, 1185-1194 (2017).
36. Bray, N.L., Pimentel, H., Melsted, P. & Pachter, L. Near-optimal probabilistic RNA-seq quantification. *Nat Biotechnol* **34**, 525-527 (2016).
37. Subramanian, A.*, et al.* Gene set enrichment analysis: a knowledge-based approach for interpreting genome-wide expression profiles. *Proc Natl Acad Sci U S A* **102**, 15545-15550 (2005).
38. Mechawar, N. & Savitz, J. Neuropathology of mood disorders: do we see the stigmata of inflammation? *Transl Psychiatry* **6**, e946 (2016).
39. Hamidi, M., Drevets, W.C. & Price, J.L. Glial reduction in amygdala in major depressive disorder is due to oligodendrocytes. *Biol Psychiatry* **55**, 563-569 (2004).
40. Bowley, M.P., Drevets, W.C., Ongur, D. & Price, J.L. Low glial numbers in the amygdala in major depressive disorder. *Biol Psychiatry* **52**, 404-412 (2002).
41. Rubinow, M.J.*, et al.* Basolateral amygdala volume and cell numbers in major depressive disorder: a postmortem stereological study. *Brain Struct Funct* **221**, 171-184 (2016).
42. Tolias, K.F., Duman, J.G. & Um, K. Control of synapse development and plasticity by Rho GTPase regulatory proteins. *Prog Neurobiol* **94**, 133-148 (2011).
43. Sibille, E.*, et al.* A molecular signature of depression in the amygdala. *Am J Psychiatry* **166**, 1011-1024 (2009).
44. Chen, L.*, et al.* MeCP2 binds to non-CG methylated DNA as neurons mature, influencing transcription and the timing of onset for Rett syndrome. *Proc Natl Acad Sci U S A* **112**, 5509-5514 (2015).
45. Roadmap Epigenomics, C.*, et al.* Integrative analysis of 111 reference human epigenomes. *Nature* **518**, 317-330 (2015).
46. Du, J., Johnson, L.M., Jacobsen, S.E. & Patel, D.J. DNA methylation pathways and their crosstalk with histone methylation. *Nat Rev Mol Cell Biol* **16**, 519-532 (2015).
47. Lister, R.*, et al.* Hotspots of aberrant epigenomic reprogramming in human induced pluripotent stem cells. *Nature* **471**, 68-73 (2011).
48. Labonte, B.*, et al.* Genome-wide epigenetic regulation by early-life trauma. *Arch Gen Psychiatry* **69**, 722-731 (2012).
49. Zhang, T.Y.*, et al.* Environmental enrichment increases transcriptional and epigenetic differentiation between mouse dorsal and ventral dentate gyrus. *Nat Commun* **9**, 298 (2018).

50. Klempan, T.A., Ernst, C., Deleva, V., Labonte, B. & Turecki, G. Characterization of QKI gene expression, genetics, and epigenetics in suicide victims with major depressive disorder. *Biol Psychiatry* **66**, 824-831 (2009).
51. Levey, D.F.*, et al.* Towards understanding and predicting suicidality in women: biomarkers and clinical risk assessment. *Mol Psychiatry* **21**, 768-785 (2016).
52. Naudin, M.*, et al.* Perceptive biases in major depressive episode. *PLoS One* **9**, e86832 (2014).
53. Huveneers, S. & Danen, E.H. Adhesion signaling - crosstalk between integrins, Src and Rho. *J Cell Sci* **122**, 1059-1069 (2009).